Gain, differential gain and linewidth enhancement factor of GaInNAs/GaAs strained quantum well lasers

2002 J. Phys.: Condens. Matter 14 3523

(http://iopscience.iop.org/0953-8984/14/13/310)

INSTITUTE OF PHYSICS PUBLISHING JOURNAL OF PHYSICS: CONDENSED MATTER

J. Phys.: Condens. Matter **14** (2002) 3523–3536 PII: S0953-8984(02)28934-1

Gain, differential gain and linewidth enhancement factor of GaInNAs/GaAs strained quantum well lasers

Dimitris Alexandropoulos and Mike J Adams

Electronics Systems Engineering Department, University of Essex, Wivenhoe Park, Colchester, Essex, CO4 3SQ, UK

Received 19 September 2001
Published 22 March 2002
Online at stacks.iop.org/JPhysCM/14/3523

Abstract

We present calculations of the material gain, differential gain and linewidth enhancement factor (alpha) for GaInNAs/GaAs quantum wells based on the free-carrier theory. We explore the effect of N composition on peak differential gain and transparency concentration. The nitrogen-induced conduction band non-parabolicity is accounted for through the band anti-crossing model, and valence band mixing effects and strain are treated exactly. The alpha factor is found to have similar values to those of the conventional material InGaAsP/InP, which is encouraging for the use of GaInNAs as the active material for a high speed emitter.

(Some figures in this article are in colour only in the electronic version)

1. Introduction

The GaInNAs/GaAs material system was first proposed and grown by Kondow *et al* [1] as an alternative material to InGaAsP, for semiconductor emitters at the important telecommunications window of 1.3 μm. This has since been demonstrated by a number of research groups [2–5]. Although laser loss mechanisms such as Auger recombination can be tackled in the conventional InP-based material by the application of strain [6], undesirable temperature-dependent effects such as heterobarrier carrier leakage at high temperatures remain. This difficulty can be overcome by using the GaInNAs material, which makes it a strong candidate for an *uncooled* emitter at 1.3 μm. In addition, vertical cavity surface emitting laser (VCSEL) fabrication technology will benefit from the use of GaInNAs quaternary. In conventional VCSELs, pairs of InP/InGaAsP layers are used for the fabrication of distributed Bragg reflectors (DBRs). These have the disadvantage of low refractive contrast, and therefore in order to attain high reflectivity, a large number of pairs has to be grown. This requires very precise control of growth to achieve DBRs with uniform thickness. On the other hand, GaInNAs allows us to use well-established high refractive index contrast GaAs/AlAs DBRs, thus making fabrication easier.

0953-8984/02/133523+14$30.00

The importance of this material lies in the unusual physical properties of III–N–V alloys compared to conventional materials (such as the widely used InGaAsP/InP). In particular, while conventional semiconductors have the tendency of increasing bandgap energy with decreasing lattice constant, III–N–V exhibit quite different behaviour: until the N content in GaNAs of 0.5, an increase of N content causes a monotonic decrease of the bandgap, instead of an increase, toward that of cubic GaN [7]. In addition, this monotonic decrease is quite abrupt and thus the bowing parameter of the III–N–V alloys is very large compared to other alloys. The underlying physical reason for this is the large difference in the electronegativity and atom size of the constituent atoms [8].

Exploiting the above-mentioned phenomenon, very deep quantum wells (QWs) can be grown on GaAs (a well-established material in optoelectronics), which will prevent carrier leakage from the heterobarrier at high temperatures. Although GaNAs is not lattice matched to GaAs, with the incorporation of In lattice-matched structures can be grown pseudomorphically on a GaAs substrate. The large bowing parameter along with strain can be combined to tailor potential device performance.

As far as theoretical investigations are concerned, a number of approaches have been adopted for the description of the physical properties of the alloy ranging from complicated band structure calculations to simpler phenomenological models. Of particular importance is the recently proposed band anti-crossing (BAC) model [9] since, despite its simplicity, it manages to explain the basic properties of the material and to provide analytical expressions, such as conduction band edge dispersion relations and electron effective mass.

As stated above, the primary use for GaInNAs/GaAs is in laser configurations. Apart from the carrier confinement a number of issues have to be addressed in order to establish this material system as a viable solution for the 1.3 μm telecommunications window. Threshold carrier densities, transparency current and spectral linewidth are some of the issues to be investigated. A measure of the spectral linewidth is the linewidth enhancement factor, alpha [10], and the functional form of the dependence is [11] $\Delta v = \Delta v_{ST}(1 + \alpha^2)$ where α is the linewidth enhancement factor and Δv_{ST} is the linewidth predicted by the modified Schawlow–Townes formula. It is our aim in this paper to study the material gain and the linewidth enhancement factor of GaInNAs/GaAs structures in the context of the BAC model.

The remainder of the paper is organized as follows. In section 2 we present a brief review of the BAC model and comment on the various parameters that are used in the model. In section 3 we calculate the band structure of GaInNAs/GaAs QWs and the transition matrix elements. In section 4 we calculate the material gain based on the free-carrier theory, taking into consideration valence band mixing effects. In section 5 we use the gain model to calculate the alpha factor for GaInNAs/GaAs single QWs and compare the results to the alpha factor for InGaAsP/InP. We also calculate the peak differential gain and transparency concentrations for various nitrogen compositions. In section 6 we discuss the results and draw some conclusions regarding the properties and the potential of this material.

2. The band anti-crossing model

As mentioned in the introduction, the band structure of III–N–V alloys has been studied using accurate calculations. Although these approaches treat the underlying physics in a systematic and accurate way, they are complicated and do not provide simple phenomenological expressions for the band structure, as needed for laser modelling. The solution to this problem is given by Shan *et al* [9] and their BAC model, which we summarize here.

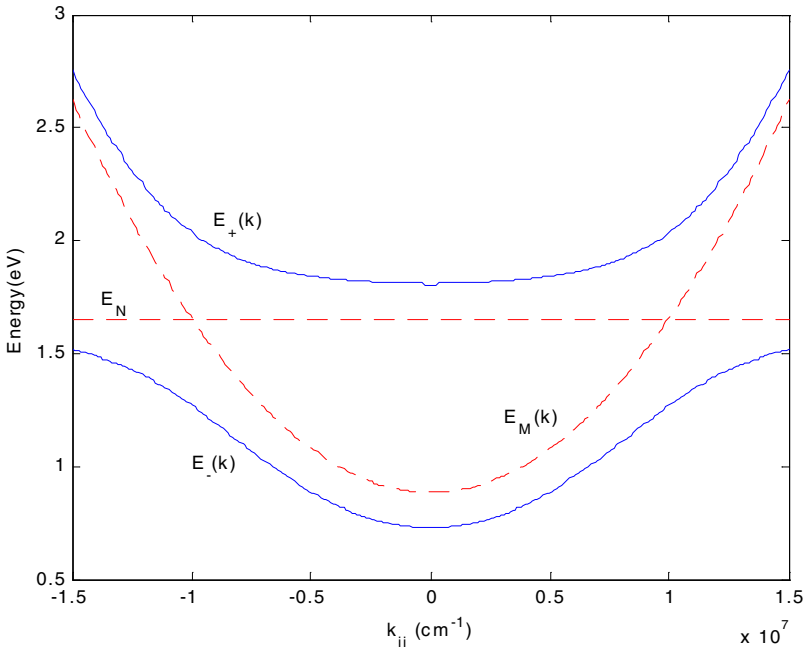

Figure 1. Schematic diagram of the band structure of the GaInNAs alloy, according to the BAC model.

2.1. The model

According to BAC, the incorporation of N into GaInAs (or GaAs) alloys leads to a strong interaction between the conduction band and a narrow resonant band formed by the N states (because of the highly localized nature of the perturbation induced by the N atoms). The overall effect is the splitting of the conduction band, with a consequent reduction of the fundamental bandgap due to the lowering of the conduction band edge.

The mathematical formalism of the model is derived as follows. The interaction between the extended conduction states of the matrix semiconductor (GaInAs) and the localized N states is treated as a perturbation which leads to the following eigenvalue problem

$$\begin{vmatrix} E - E_{\mathrm{M}} & -V_{\mathrm{MN}} \\ -V_{\mathrm{MN}} & E - E_{\mathrm{N}} \end{vmatrix} = 0 \tag{1}$$

where E_{M} are the conduction states of the matrix semiconductor, E_{N} are the localized states of the nitrogen, and V_{MN} is the matrix element describing the interaction between E_{M} and E_{N}. It is V_{MN} that leads to the mixing and anti-crossing of these two states. The solution to the eigenvalue problem (1) gives the dispersion relations for GaInNAs

$$E(k)_{\pm} = \frac{E_{\mathrm{N}} + E_{\mathrm{M}}(k) \pm \sqrt{(E_{\mathrm{N}} - E_{\mathrm{M}}(k))^2 + 4V_{\mathrm{MN}}^2}}{2}. \tag{2}$$

A schematic diagram of the band structure for GaInNAs according to equation (2), and the $E_{\mathrm{M}}(k)$ and E_{N} levels, is shown in figure 1. The states of the subbands are represented by functions that are a mixture of extended conduction band and localized nitrogen states.

2.2. Verification of the band anti-crossing model

In the literature it seems, so far, that the BAC model is well established as far as the macroscopic behaviour is concerned. Shan *et al* [9, 12] measured optical transitions under pressure, where optical transitions are observed which are associated with the two branches of the split lowest conduction band in GaInNAs and GaNAs for various compositions. This involved photomodulation reflectance spectra from $Ga_xIn_{1-x}N_yAs_{1-y}$ and GaN_xAs_{1-x} where the repulsion of the two levels (E_+ and E_- as shown in figure 1) with nitrogen composition was observed, thus explaining the observed redshift of the bandgap energy with increasing N content.

Skierbiszewski *et al* [13] examined the carrier dynamics in a GaNAs alloy where they measured the mobility of carriers in the alloy and compared it to the theoretical mobility, calculated, from the BAC model; the qualitative and quantitative agreement of theory and experiment was good. These authors also examined the increase of the conduction band effective mass theoretically (in the context of the BAC model) and experimentally; again the agreement was very good [14].

Uesugi *et al* [15] have indirectly confirmed the central idea of the model (i.e. the interaction of the extended and localized levels) through the temperature dependence of bandgap energies of GaNAs films for various N concentrations. The result showed that, in determining the temperature dependence of the bandgap energy, two kinds of N-related energy states with different temperature dependence of bandgap energy must be considered: one with a higher temperature dependence similar to the GaAs bands (extended like state) and an N-related localized state with lower temperature dependence.

Finally, Lindsay and O'Reilly [16] have adopted a theoretical approach. By using a tight-binding sp^3s^* Hamiltonian, they have calculated the compositional dependence of the conduction band edge and then compared it with the E_- energy calculated according to the BAC model. The results were found to be in good agreement.

2.3. Important parameters within the BAC model: V_{MN}, E_N and electron effective mass

In order for the dispersion relation predicted by the model to reproduce the band structure of the real semiconductor as accurately as possible, the interaction matrix element V_{MN} and the nitrogen level E_N must be determined along with their dependence on composition. In addition, an accurate form for the electron effective mass is required for the calculation of various laser parameters. V_{MN} and E_N have been treated experimentally by Shan *et al* [9, 12] and Skierbiszewski *et al* [13] (by treating V_{MN} as a fitting parameter to the experimental results) and theoretically by Lindsay and O'Reilly [16]. The net result is that V_{MN} increases with the increase of the N composition. Some indicative values are $V_{MN} = 0.12$ eV for $x = 0.009$ and $V_{MN} = 0.4$ eV for $x = 0.023$. It should be noted that the In concentration was fixed at 0.08. The functional form derived by Lindsay and O'Reilly is the following

$$V_{MN} = C_{MN}\sqrt{x} \tag{3}$$

and for GaNAs they have determined theoretically $C_{MN} = 1.50$. E_N is found to vary as

$$E_N = E_N^o - \gamma x \tag{4}$$

where $E_N^o = 1.675$ eV and $\gamma = 2.52$.

The electron effective mass and its dependence on the nitrogen concentration has been studied by Lindsay and O'Reilly [16] who derived the form of the electron effective mass using $\boldsymbol{k} \cdot \boldsymbol{p}$ band structure calculations. It was found that the effective mass increases with nitrogen

concentration up to a limit above which it will decrease. According to the BAC model, the mass is derived from the conduction band dispersion relation

$$m(E) = m_e^m \left[1 + \left(\frac{V_{\mathrm{MN}}}{E_{\mathrm{N}} - E} \right)^2 \right] \tag{5}$$

where m_e^m is the conduction band effective mass of the ternary GaInAs. This functional form of the mass has been used by Skierbiszewski *et al* [13] to model the experimental results. Again, it is predicted that the mass will increase with the increase of nitrogen composition but, contrary to the findings of Lindsay and O'Reilly, it will increase monotonically with concentration. However, despite this discrepancy in the trends it is well established theoretically and experimentally that the effective mass of GaInNAs or GaNAs is very large compared to other alloys used in optoelectronics.

3. Band structure of GaInNAs

The band structure of GaInNAs has been studied before, employing a 10×10 Hamiltonian considering the coupling of the conduction and valence bands [17] and the effect of the coupling of the nitrogen band to the valence band [18]. For the needs of the present approach, the conduction bands are taken to be decoupled from the valence bands, which is a valid approximation given that the emission wavelength of interest is 1.3 μm. Thus the inclusion of the coupling between the conduction bands and valence bands will induce a minor correction [19]. Hence the study of the trends of optical properties is possible with a simpler model.

For the calculation of the conduction band structure, the coupling of the extended like states and the nitrogen states is considered through the BAC model presented above and the envelope function approximation. For the calculation of the valence band structure we have used a 6×6 Hamiltonian accounting for the spin orbit effects. This is further block diagonalized under the axial approximation, thus reducing the dimensionality of the matrix to 3×3. The strain-dependent coupling of the heavy hole (HH), light hole (LH), and spin–orbit split-off (SO) valence subbands is accounted for in the context of the deformation potential theory as described in [20].

The parameters for the quaternary compounds, such as Luttinger parameters, lattice constants and strain-related parameters, are obtained by the linear interpolation between the values of the binary compounds found in [21]. For the nitrogen-related binaries the values correspond to the cubic form of these.

Both schemes are solved numerically using a finite difference approach. The boundary conditions and the Hermitian properties of the Hamiltonian are obtained using the finite difference formulae found in [22]. It is important to note that, for the numerical calculation under the finite difference scheme, special care must be taken in the number of subsections of the barrier and well regions considered to ensure the stability of the results. In our case this was 60. In the remaining calculations we consider a device with a GaInNAs well of 6 nm width surrounded by 7 nm GaAs barriers.

The matrix element V_{MN} and the nitrogen level dependence on the nitrogen composition are [17] $V_{\mathrm{MN}} = 2.4\sqrt{x}$ and $E_{\mathrm{N}} = 1.52\ \mathrm{eV} - 3.9x$, respectively. The conduction band energy E_{M} of the matrix semiconductor is taken to vary in the presence of nitrogen as $E_{\mathrm{M}} = E_0 - 1.55x$ where E_0 is the energy in the absence of nitrogen.

Figure 2 shows the band structure of a 6 nm compressively strained ($\varepsilon = -0.82\%$) $Ga_{0.8}In_{0.2}N_{0.03}As_{0.97}$/GaAs single QW (solid curves). The band structure exhibits the usual trends expected for compressively strained materials. For the sake of comparison we

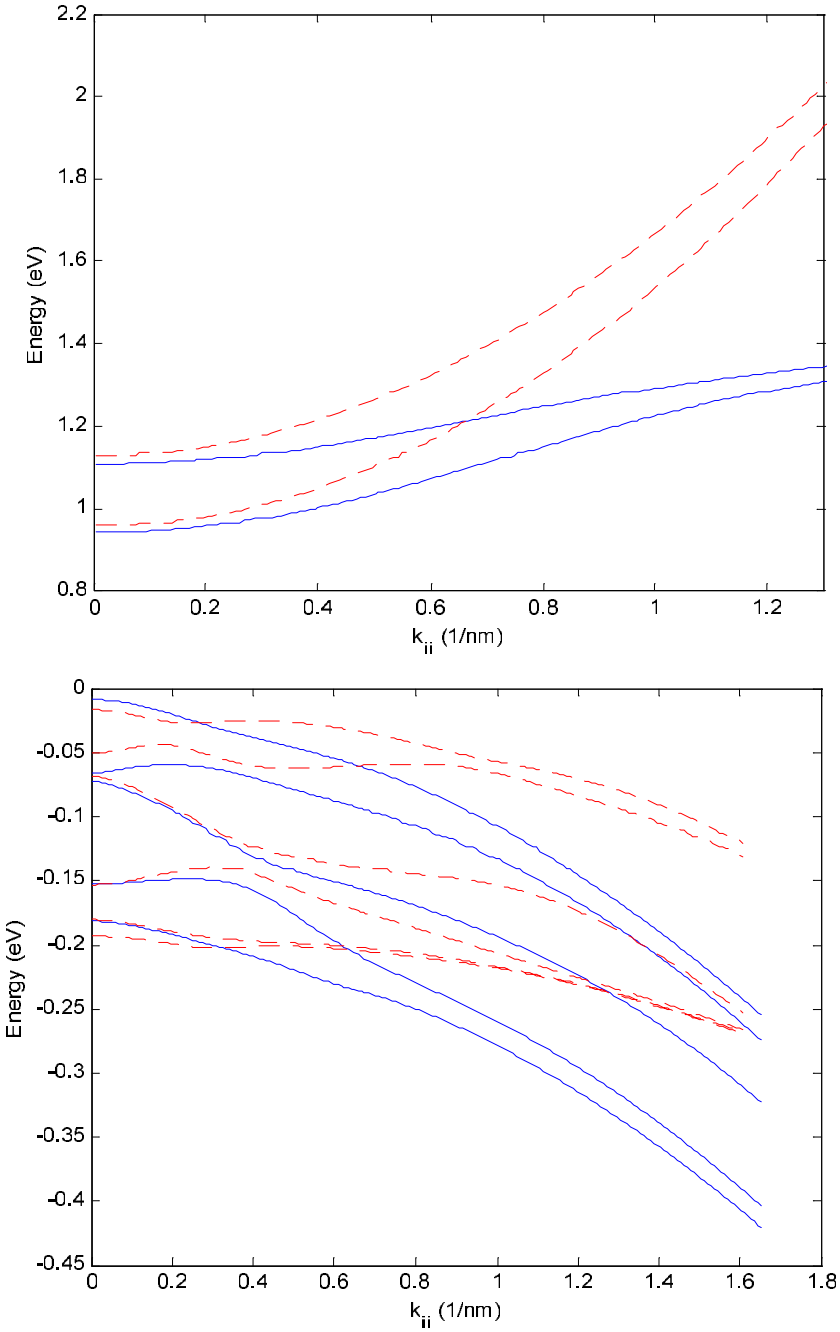

Figure 2. (a) Conduction band and (b) valence band structures for a 6 nm $Ga_{0.8}In_{0.2}N_{0.03}As_{0.97}$/GaAs single QW (solid curves) and 6 nm $In_{0.7}Ga_{0.3}As_{0.72}P_{0.28}$/InP (dashed curves).

have also calculated the band structure of 6 nm compressively strained ($\varepsilon = -0.24\%$) $In_{0.7}Ga_{0.3}As_{0.72}P_{0.28}$/InP (dashed curves). The band edge electron effective mass for the lower

subbands for the two materials does not differ significantly but it is evident that the average effective mass is larger in GaInNAs. As discussed later, this affects the subband carrier populations and may prove a beneficial characteristic for device design issues.

4. Gain calculations

In this section we calculate the material gain using the parameters predicted from the BAC model presented above and accounting for the valence band mixing effects through the 6×6 Hamiltonian. We have adopted an approach based on Fermi's golden rule. More complicated gain calculations that take into account many body effects can be found elsewhere [17,23]. The many body approach has the benefit of not requiring dephasing times, and the gain curves have better agreement with the experimental results, with consequent changes in the differential gain and alpha. In this contribution we want to highlight the effects of the unusual band structure of GaInNAs, hence it is sufficient to simplify the approach by neglecting the Coulombic effects and accounting for recombination through the free-carrier theory.

The material gain of a QW, including the valence band mixing effects and a Lorentzian lineshape, is given by the following relation [22]

$$g(E) = \frac{q^2\pi}{n_{\mathrm{r}} c\varepsilon_o m_o^2 \omega L_z} \sum_{\eta=\uparrow,\downarrow} \sum_{\sigma=U,L} \sum_{n,m} \int \left|\hat{e} M_{nm}^{\eta\sigma}(k_t)\right|^2 \frac{(f_n^c(k_t) - f_{\sigma m}^v(k_t))(\hbar/\tau)}{(E_{\sigma,nm}^{cv}(k_t) - E)^2 + (\hbar/\tau)^2} \frac{k_t \mathrm{d}k_t}{2} \tag{6}$$

where

$$\begin{aligned} f_n^c(k_t) &= \frac{1}{1 + \exp\left(\frac{E_n^c(k_t) - E_{fc}}{k_{\mathrm{B}}T}\right)} \\ f_{\sigma m}^v(k_t) &= \frac{1}{1 + \exp\left(\frac{E_{\sigma m}^v(k_t) - E_{fv}}{k_{\mathrm{B}}T}\right)} \\ E_{\sigma,nm}^{cv}(k_t) &= E_n^c(k_t) - E_{\sigma,m}^v(k_t) \end{aligned} \tag{7}$$

where E_{fc} and E_{fu} are the quasi-Fermi levels of the electrons and holes respectively, n_{r} is the refractive index of the well material, L_z is the well width, $\hat{e}$ is the polarization vector, τ is the intraband relaxation time, $M_{nm}^{\eta\sigma}(k_t)$ is the momentum matrix element, and the other symbols have their usual meaning. The index η in the summations accounts for the spin, σ for the upper and lower part of the block diagonalized Hamiltonian each of dimension 3×3 and n, m for the quantized states in the conduction and valence band respectively.

The momentum matrix element is given by $M_{nm}^{\eta\sigma}(k_t) = \left\langle \Psi_{m,k_t}^{v,\sigma} \middle| p \middle| \Psi_{n,k_t}^{c,\eta} \right\rangle$ where p is the momentum operator and $\Psi_{m,k_t}^{v,\sigma}$ and $\Psi_{n,k_t}^{c,\eta}$ are the wavefunctions of the valence and conduction band states, respectively, as calculated by the 6×6 Hamiltonian for the valence band states and by the 2×2 Hamiltonian for the conduction band states.

The momentum matrix elements for the TE and TM polarizations are given by:

$$\begin{aligned} |M_{\mathrm{TE}}|^2 &= \left|\hat{x} M_{nm}^{\eta\sigma}(k_t)\right|^2 = \left|\hat{y} M_{nm}^{\eta\sigma}(k_t)\right|^2 = \frac{M_{\mathrm{b}}^2}{4}\left\{\left|\left\langle g_{m,lh}^{\sigma} + \sqrt{2} g_{m,so}^{\sigma} \middle| \phi_n \right\rangle\right|^2 + 3\left|\left\langle g_{m,hh}^{\sigma} \middle| \phi_n \right\rangle\right|^2\right\} \\ |M_{\mathrm{TM}}|^2 &= \left|\hat{z} M_{nm}^{\eta\sigma}(k_t)\right|^2 = M_{\mathrm{b}}^2\left|\left\langle g_{m,lh}^{\sigma} - (1/\sqrt{2}) g_{m,so}^{\sigma} \middle| \phi_n \right\rangle\right|^2 \end{aligned} \tag{8}$$

where $g_{m,lh}^{\sigma}$, $g_{m,hh}^{\sigma}$, $g_{m,so}^{\sigma}$ and ϕ_n are the envelope functions of the LH, HH, SO and conduction band states, respectively; that is, the eigenvectors of the 6×6 Hamiltonian for the valence band states and the 2×2 Hamiltonian for the conduction band states. M_{b} is the bulk value of the momentum matrix element given by $M_{\mathrm{b}}^2 = m_o E_{\mathrm{P}}/6$ where E_{P} is an energy parameter which can be calculated from a linear interpolation scheme from the binary semiconductors. The values of E_{P} are taken from [21].

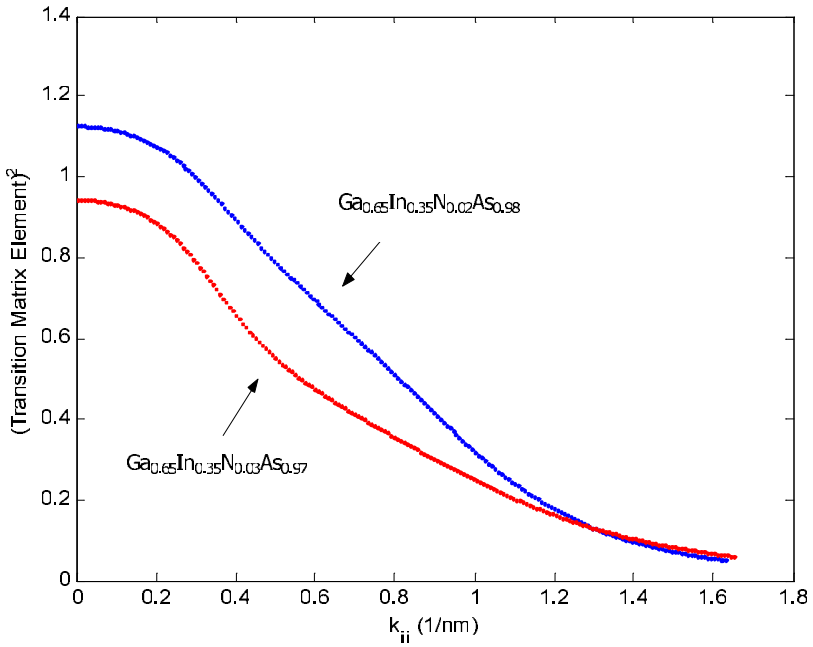

Figure 3. TE transition matrix element for the lower transition (C1→ HH1) for a 6 nm GaInNAs/GaAs single QW for the compositions shown.

In our calculations we have assumed a minimal overlap between the nitrogen-related states and the extended like states of the valence bands, given the strong localization of the former. Indeed, in the relations above, ϕ_n are the envelope functions corresponding to the extended like part of the conduction band wavefunction. The transition matrix element given the above-mentioned assumption is a factor that now has to be taken into account when considering the design of optoelectronic devices based on GaInNAs. This is so because with increasing nitrogen composition the localized part of the conduction band is enhanced leading to a reduced transition matrix element. This can be seen in figure 3 which shows the C1→ HH1 TE transition matrix element for two different nitrogen concentrations. The effect of the transition matrix element on design issues is considered further in [24].

Figure 4 shows the optical material gain spectrum for GaInNAs for various carrier concentrations. For these calculations we have considered that the N-induced redshift of the bandgap is mainly accommodated by the conduction band offset, namely 75% and allowing for 25% in the valence band. This is in agreement with [17]. However it has been suggested that the incorporation of N causes the lowering of not only the conduction band edge, but also the valence band edge [7], which will effectively lead to type II alignment. The same discrepancy also exists in theoretical works. In particular for the GaNAs/GaAs material system, early work [25] favoured the type II alignment, whereas more recent theoretical work [26] suggests a type I alignment. The latter has been observed recently [27]. It should be emphasized that the gain calculations are sensitive to the band offsets considered [28].

The calculation is made for well width $L = 6$ nm, In concentration of 20% and N concentration of 2.9%. The carrier concentrations are 1.84×10^{12}, 2.2×10^{12}, 2.53×10^{12} and 2.9×10^{12} cm^{-2}, and the intraband relaxation time is taken as $\tau = 0.1$ ps. The negative values of gain below the bandgap are a well-known result of the Lorentzian lineshape function.

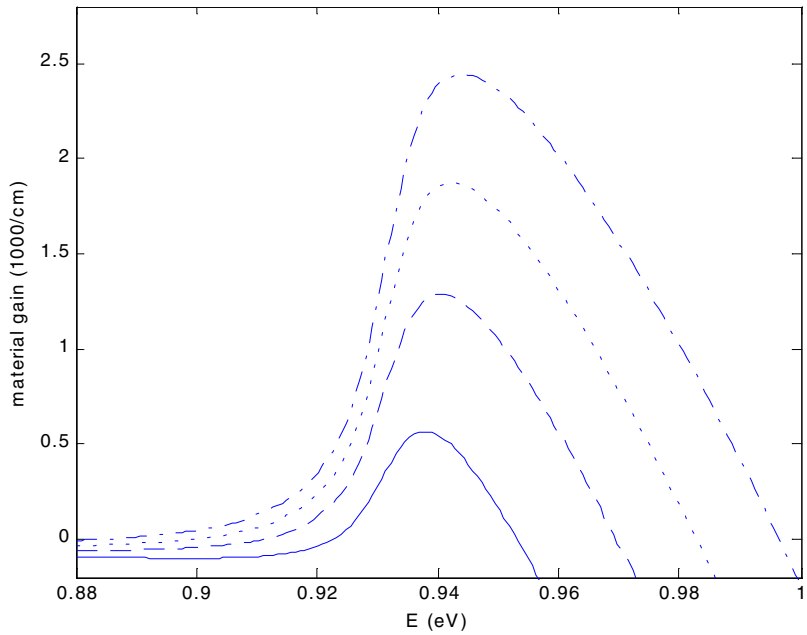

Figure 4. Material gain for a 6 nm $Ga_{0.8}In_{0.2}N_{0.03}As_{0.97}$/GaAs single QW for the following concentrations (in increasing order): 1.84×10^{12} cm^{-2} (solid curve); 2.2×10^{12} cm^{-2} (dashed curve); 2.53×10^{12} cm^{-2} (dotted curve); and 2.9×10^{12} cm^{-2} (dashed dotted curve).

5. Alpha factor

Having established a model for the gain of GaInNAs/GaAs in the context of the BAC model, we can proceed with the calculation of the linewidth enhancement factor (alpha factor) and investigate the implications of the higher effective mass. Accounting for valence band mixing effects, the expression [29] used here is

$$a(E) = \frac{\sum_{\eta=\uparrow,\downarrow}\sum_{\sigma=U,L}\sum_{n,m}\int \left|\hat{e}M^{\eta\sigma}_{nm}(k_t)\right|^2\left(\frac{\mathrm{d}f^c_n(k_t)}{\mathrm{d}N}-\frac{\mathrm{d}f^v_{\sigma m}(k_t)}{\mathrm{d}N}\right)\frac{E-E^{cv}_{\sigma,nm}(k_t)}{(E^{cv}_{\sigma,nm}(k_t)-E)^2+(\hbar/\tau)^2}k_t\,\mathrm{d}k}{\sum_{\eta=\uparrow,\downarrow}\sum_{\sigma=U,L}\sum_{n,m}\int \left|\hat{e}M^{\eta\sigma}_{nm}(k_t)\right|^2\left(\frac{\mathrm{d}f^c_n(k_t)}{\mathrm{d}N}-\frac{\mathrm{d}f^v_{\sigma m}(k_t)}{\mathrm{d}N}\right)\frac{(\hbar/\tau)}{(E^{cv}_{\sigma,nm}(k_t)-E)^2+(\hbar/\tau)^2}k_t\,\mathrm{d}k} \tag{9}$$

where the numerator is the Kramers–Kronig transform of the denominator. The denominator represents the differential gain whereas the numerator is related to the change of the real part of the refractive index with the injected carrier density. Alternatively, expression (9) can be interpreted [29] as the ratio of the FM modulation index to the AM modulation index.

We have calculated the linewidth enhancement factor for $Ga_{0.66}In_{0.34}N_{0.021}As_{0.98}$/GaAs and $In_{0.7}Ga_{0.3}As_{0.72}P_{0.28}$/InP. The width of the QW in both material systems is 6 nm. Both are calculated for 1.58×10^{12} cm^{-2} carrier concentration and the intraband relaxation time is taken as $\tau = 0.1$ ps. The results are shown in figure 5 and the differential gain is shown in figure 6 for the two material systems.

In order to clarify the effect of the nitrogen concentration on the differential gain we have calculated the peak differential gain and transparency concentrations for five combinations of In and N content for a 7.1 nm GaInNAs/GaAs QW such that the emission wavelength is approximately 1.3 μm. The peak differential gain is shown in figure 7, and figure 8 shows the change of the transparency concentrations with N content for each case.

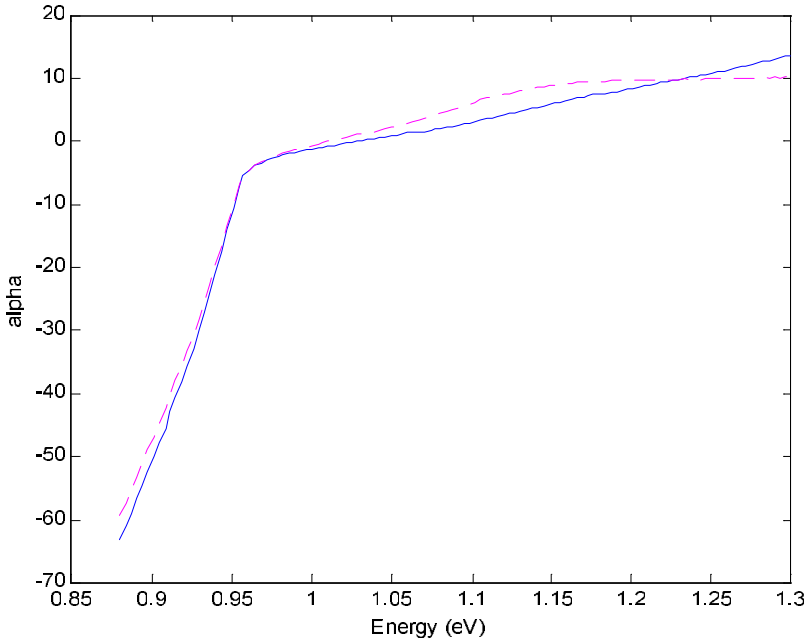

Figure 5. Alpha factor for a 6 nm $Ga_{0.66}In_{0.34}N_{0.021}As_{0.98}$/GaAs single QW (solid curve) and 6 nm $In_{0.7}Ga_{0.3}As_{0.72}P_{0.28}$/InP (dashed curve).

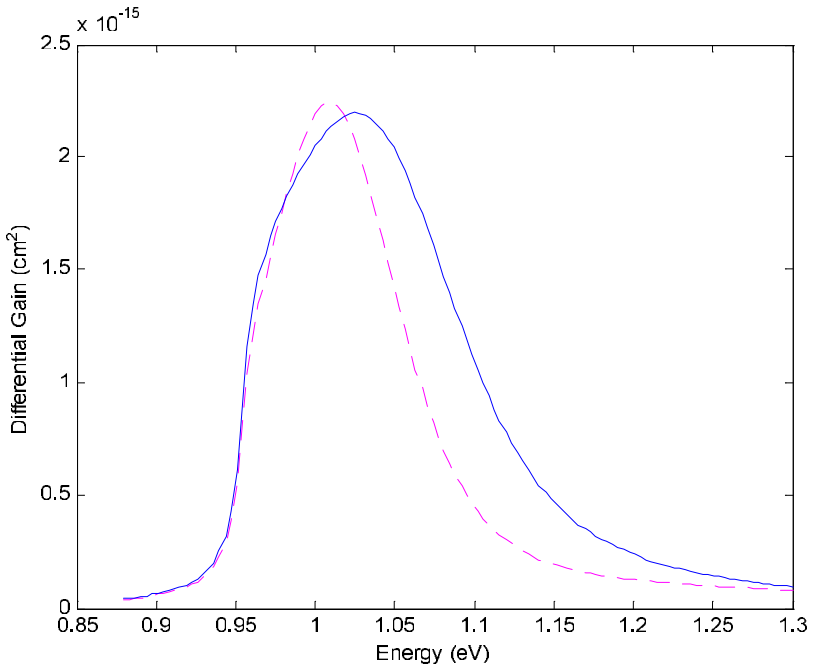

Figure 6. Differential gain for a 6 nm $Ga_{0.66}In_{0.34}N_{0.021}As_{0.98}$/GaAs single QW (solid curve) and 6 nm $In_{0.7}Ga_{0.3}As_{0.72}P_{0.28}$/InP (dashed curve).

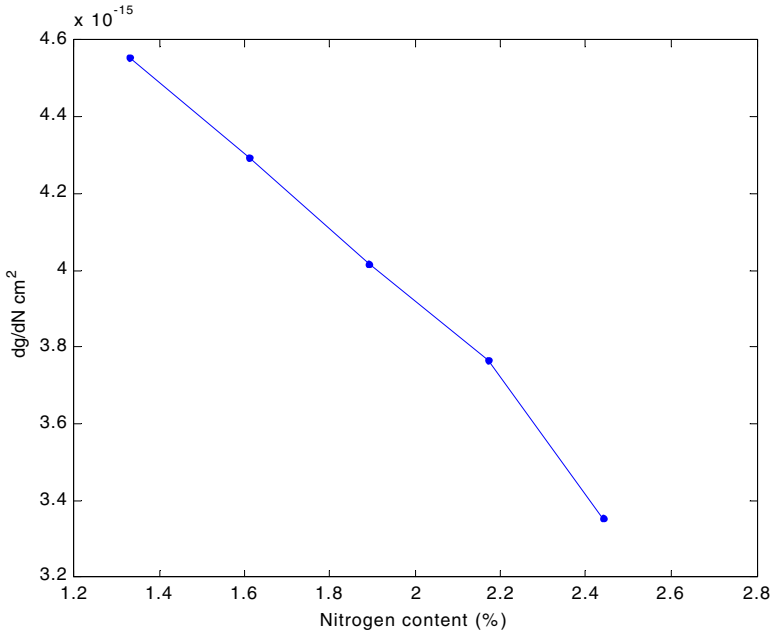

Figure 7. Peak differential gain with nitrogen composition.

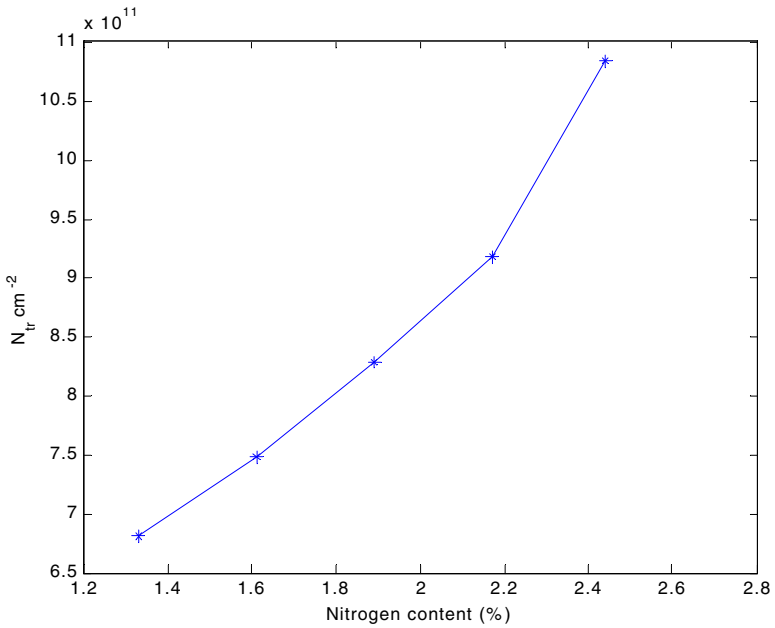

Figure 8. Transparency concentration with nitrogen composition.

6. Discussion

The dispersion of alpha has the typical form found elsewhere [30], i.e. it increases with photon energy starting from negative values and becoming positive. The latter follows the dispersion

of the change of refractive index with carrier concentration. As shown in figure 5 the alpha factor, as calculated in the context of the BAC model, does not differ significantly from that of InGaAsP/InP. This indicates that GaInNAs/GaAs will be suitable for transmitters in high-speed transmission systems. Given the square dependence of the linewidth on alpha factor (see section 1), for the use of GaInNAs as a light emitter, one is mainly concerned with values of alpha near the zero point. Therefore the operation wavelength should be tailored so that it is in this region. The performance and the alpha factor can be further optimized by tailoring the compressive strain [31].

It is evident from figure 6 that the bandwidth of the differential gain of GaInNAs is broader compared to that of InGaAsP, whereas the peak value slightly smaller for the given concentrations. As far as the peak value is concerned, it is not our intention in this paper to draw any conclusions relative to the InGaAsP/InP materials since these will be blurred by the fact that the peak value is strongly dependent on the quantum confinement effect and strain, as discussed elsewhere [32]. However, the enhanced bandwidth of the differential gain spectrum is a direct implication of the conduction band non-parabolicity of GaInNAs alloys which results in the high electron effective mass.

Apart from the superior temperature performance which is an experimentally confirmed property of the GaInNAs/GaAs alloys and originates from the hybrid nature of the conduction band states (mixture of atomic like states with extended like states), another important parameter is the higher electron effective mass of GaInNAs/GaAs alloys. It is our aim at this point to discuss the influence that this has on design issues. It is well established both experimentally and theoretically (despite the difference in the predicted trends) that the electron effective mass of GaInNAs is considerably higher than in GaInAs. Some indicative values are $m_e = 0.13m_o$ for $Ga_{0.93}In_{0.07}N_{0.02}As_{0.98}$ (see, for example, [33]) and $m_e = 0.08m_o$ for $Ga_{0.62}In_{0.38}N_{0.015}As_{0.985}$ (see, for example, [34]). Extending our study further in k-space, in terms of an average effective mass this will be high in GaInNAs. This will reduce the differential gain as shown in figure 7. The effect of the higher electron effective mass of GaInNAs on the peak differential gain can be further understood in terms of the increased density of states. Indeed, a high electron effective mass translates to a higher density of states. Therefore, the quasi-Fermi level moves slowly with injected carriers, leading to decreased peak differential gain.

The above comments, however, have to be considered in conjunction with the valence and conduction subband spacing and the reduced transition matrix element. As shown in figure 2(a), the valence band structure of GaInNAs exhibits a lower density of states, compared to InGaAsP, and higher subband spacing. Therefore the implications of the high electron effective mass will be compensated and controlled by the valence band structure. This argument provides a simple design guideline. Given that maximum differential gain is desirable for a laser structure, one should aim to achieve the wavelength of emission with the maximum In percentage allowed by the growth technique. In this way compressive strain is enhanced resulting in the repulsion of the valence bands, thus leading to the increase of the subband spacing. As far as the conduction band is concerned, the portion of the extended like states involved in the formation of the band states is enhanced with a consequent increase in the overlap integral and therefore an increase in the peak gain.

In band structure terms, the high electron effective mass translates to more symmetrical conduction and valence bands, compared to conventional material systems where the electron effective mass is much smaller than the hole effective mass. This symmetry is evident further from the band edge in the context of the BAC model. Therefore the injected carriers are more symmetrically distributed in the bands compared to conventional laser structures. This is reflected in the more symmetrical shift of the Fermi levels for the electron and holes with

carrier concentrations. However this will not induce a decrease in the transparency since, although the Fermi levels move more symmetrically with carrier concentration, the higher density of states in the conduction band delays this change (this is shown in figure 8). It is clear that symmetrical bands do not imply reduced transparency. Therefore, when considering transparency concentration, the bands should be engineered in such a way that the overall effect is the reduced value of the density of states in both bands.

7. Conclusion

We have calculated the optical gain and linewidth enhancement factor for 1.3 μm GaInNAs/GaAs QWs in the context of the BAC model including valence band mixing. We have also explored the effect of N composition on important properties such as the differential gain and the transparency concentration. We have also made a qualitative study of the effect of the electron effective mass in this alloy. An increase of N content reduces the peak differential gain and increases the transparency concentration, therefore the route of high In fraction and low N fraction should be followed when designing an emitter. Given the fact that the linewidth enhancement factor of GaInNAs/GaAs does not differ significantly from that of InGaAsP/InP, it can be concluded that GaInNAs possesses the spectral characteristics for a high-speed transmitter. Thus this material system seems a viable solution for the 1.3 μm telecommunications window.

Acknowledgments

We would like to acknowledge S L Chuang and P Enders for helpful discussions on the band structure calculations and M Silver for helpful comments on the manuscript. One of us (DA) would like to acknowledge Agilent Technologies (UK) and EPSRC (UK) for financial support. This work is supported under an EPSRC research project.

References

[1] Kondow M, Uomi K, Niwa A, Kitatani T, Watahiki S and Yazawa Y 1996 GaInNAs: a novel material for long-wavelength-range laser diodes with excellent high-temperature performance *Japan. J. Appl. Phys.* **35** 1273–5

[2] Nakahara K, Kondow M, Kitatani T, Larson M C and Uomi K 1998 1.3 μm continuous-wave lasing operation in GaInNAs quantum-well lasers *IEEE Photon. Technol. Lett.* **10** 487–8

[3] Sato S and Satoh S 1999 1.3 μm continuous-wave operation of GaInNAs lasers grown by metal organic chemical vapour deposition *Electron. Lett.* **35** 1251–2

[4] Hohnsdorf F, Koch J, Leu S, Stolz W, Borchert B and Druminski M 1999 Reduced threshold current densities of (GaIn)(NAs)/GaAs single QW lasers for emission wavelengths in the range 1.28–1.38 μm *Electron. Lett.* **35** 571–2

[5] Yang X, Jurkovic M J, Heroux J B and Wang W I 1999 Low threshold InGaAsN/GaAs single QW lasers grown by molecular beam epitaxy using Sb surfactant *Electron. Lett.* **35** 1081–3

[6] O'Reilly E P 1989 Valence band engineering in strained layer structures *Semicond. Sci. Technol.* **4** 121–37

[7] Kondow M, Kitatani T, Nakatsuka S, Larson M, Nakahara K, Yazawa Y, Okai M and Uomi K 1997 GaInNAs: a novel material for long-wavelength semiconductor lasers *IEEE J. Select. Top. Quantum Electron.* **3** 719–30

[8] Wei S and Zunger A 1996 Giant and composition-dependent optical bowing parameter in GaNAs alloys *Phys. Rev. Lett.* **76** 664–7

[9] Shan W, Walukiewicz W, Ager J W III, Haller E E, Geisz J, Friedman D, Olson J and Kurtz S R 1999 Band anticrossing in GaInNAs alloys *Phys. Rev. Lett.* **82** 1221–4

[10] Henry C H 1982 Theory of the linewidth of semiconductor lasers *IEEE J. Quantum Electron.* **18** 259–64

[11] Yariv A 1989 *Quantum Electronics* (New York: Wiley)

[12] Shan W, Walukiewicz W, Ager J W III, Haller E E, Geisz J, Friedman D, Olson J and Kurtz S R 1999 Effect of nitrogen on the band structure of GaInNAs alloys *J. Appl. Phys.* **86** 2349–51
[13] Skierbiszewski C *et al* 1999 Effect of nitrogen-induced modification of the conduction band structure and electron transport in GaAsN alloys *Phys. Status Solidi* b **216** 135–9
[14] Skierbiszewski C *et al* 2000 Large, nitrogen-induced increase of the electron effective mass in $In_yGa_{1-y}N_xAs_{1-x}$ *Appl. Phys. Lett.* **76** 2409–11
[15] Uesugi K, Suemune I, Hasegawa T and Akutagawa T 2000 Temperature dependence of band gap energies of GaAsN alloys *Appl. Phys. Lett.* **76** 1285–7
[16] Lindsay A and O'Reilly E P 1999 Theory of enhanced bandgap non-parabolicity in GaN_xAs_{1-x} and related alloys *Solid State Commun.* **112** 443–7
[17] Hader J, Koch S W, Moloney J V and O'Reilly E P 2000 Gain in 1.3 μm materials: InGaNAs and InGaPAs semiconductor quantum-well lasers *Appl. Phys. Lett.* **77** 630–2
[18] O'Reilly E P and Lindsay A 1999 k·P model of ordered GaN_xAs_{1-x} *Phys. Status Solidi* b **216** 131–4
[19] Chitta V A, Degani M H, Cohen A M and Marques G E 1998 Dynamic mass effects on confined exciton states *Phys. Rev.* B **38** 8533–6
[20] Chuang S L 1995 *Physics of Optolectronic Devices* (New York: Wiley-Interscience)
[21] Vurgaftman I, Meyer J R and Ram-Mohan L R 2001 Band parameters for III–V cpmpound semiconductors and their alloys *J. Appl. Phys.* **89** 5815–75
[22] Chang C and Chuang S L 1995 Modelling of strained quantum-well lasers with spin–orbit coupling *IEEE J. Select. Top. Quantum Electron.* **1** 218–29
[23] Chow W W, Jones E D, Modine N A, Allerman A A and Kurtz S R 1999 Laser gain and threshold properties in compressive-strained and lattice-matched GaInNAs/GaAs quantum wells *Appl. Phys. Lett.* **75** 2891–3
[24] Alexandropoulos D and Adams M J Design considerates for 1.3 μm emission of GaIn NAs/GaAs strained quantum well lasers in preparation
[25] Sakai S, Ueta Y and Terauchi Y 1993 Band gap energy and band lineup of III–V alloy semiconductors incorporating nitrogen and boron *Japan. J. Appl. Phys.* **32** 4413–17
[26] Bellaiche L, Wei S and Zunger A 1997 Composition dependence of interband transition intensities in GaPN, GaAsN and GaPAs alloys *Phys. Rev.* B **56** 10 233–40
[27] Buynova I A, Pozina G, Hai P N, Chen W M, Xin H P and Tu C W 2001 Type I band alignment in GaN_xAs_{1-x}/GaAs quantum wells *Phys. Rev.* B **63** 033303
[28] Hader J, Koch S W, Moloney J V and O'Reilly E P 2000 Influence of the valence-band offset on gain and absorption in GaInNAs/GaAs quantum-well lasers *Appl. Phys. Lett.* **76** 3685–7
[29] Arakawa Y and Yariv A 1985 Theory of gain, modulation response, and spectral linewidth in AlGaAs quantum well lasers *IEEE J. Quantum Electron.* **21** 1666–74
[30] Osinski M and Buus J 1987 Linewidth enhancement factor in semiconductor lasers—an overview *IEEE J. Quantum Electron.* **23** 9–29
[31] Mullane M and McInerney J G 1999 Minimization of the linewidth enhancement factor in compressively strained semiconductor lasers *IEEE Photonics Technol. Lett.* **11** 776–8
[32] Seki S and Yokoyama K 1993 Strain and quantum-confinement effects on differential gain of strained InGaAsP/InP quantum well lasers *J. Appl. Phys.* **74** 4242–4
[33] Jones E D, Modine N A, Allerman A A, Fritz I J, Kurtz S R, Rigth A F, Tozer S T and Wei X 1999 *Proc. SPIE* **52** 3621
[34] Hetterich M, Dawson M D, Egorov A Yu, Bernklau D and Riechert H 2000 Electronic states and band alignment in GalnNAs/GaAs quantum-well structures with low nitrogen content *Appl. Phys. Lett.* **76** 1030–2